The University of Akron
IdeaExchange@UAkron

Williams Honors College, Honors Research Projects

The Dr. Gary B. and Pamela S. Williams Honors College

Summer 2019

Theoretical Study of Fano Resonance in a Mechanical System

Alex Alberts
ama239@zips.uakron.edu

Please take a moment to share how this work helps you through this survey. Your feedback will be important as we plan further development of our repository.
Follow this and additional works at: https://ideaexchange.uakron.edu/honors_research_projects

Part of the Acoustics, Dynamics, and Controls Commons

Recommended Citation
Alberts, Alex, "Theoretical Study of Fano Resonance in a Mechanical System" (2019). *Williams Honors College, Honors Research Projects*. 938.
https://ideaexchange.uakron.edu/honors_research_projects/938

This Honors Research Project is brought to you for free and open access by The Dr. Gary B. and Pamela S. Williams Honors College at IdeaExchange@UAkron, the institutional repository of The University of Akron in Akron, Ohio, USA. It has been accepted for inclusion in Williams Honors College, Honors Research Projects by an authorized administrator of IdeaExchange@UAkron. For more information, please contact mjon@uakron.edu, uapress@uakron.edu.

ABSTRACT

Resonance conditions are a major area of study in theoretical and experimental investigation. Normally, a resonance condition is characterized by a symmetric shape on both sides of the resonance. In some cases, we can observe an asymmetric resonance shape, which is called a Fano resonance. We will study the appearance of Fano resonance in a purely mechanical system. The frequency response of the primary system is approximated using the method of multiple scales focusing on the location of the resonance condition. Then, curve fitting is used to approximate the Fano parameter associated with the system, which provides a measurement of the asymmetry in the resonance line-shape. Using this, we investigate how the various parameters associated with the system influence the strength of the Fano resonance.

TABLE OF CONTENTS

LIST OF FIGURES

CHAPTER I

INTRODUCTION

Resonance conditions are a major area to study in both experimental and theoretical investigation, as they show up in many different contexts. In a mechanical system, resonance conditions often result from an external force with input frequency that is close to the natural frequency of the system, which then results in large steady-state oscillations in the system. In most cases where a resonance condition appears, we observe symmetry on both sides of the resonance, and, when this is the case, the resonance line-shape is said to be Lorentzian. Also, there are cases where a destructive resonance condition appears, sometimes referred to as an anti-resonance, which is characterized by the response being supressed, rather than enchanced, when this resonance condition is met. Furthermore, there are certain cases when the resonance line-shape is asymmetric, which is called a Fano resonance, originally studied by U. Fano in the context of quantum mechanics, where a resonance and anti-resonance appear very close together [1]. Due to the various different applications of Fano resonance, which we will discuss later, we seek to further understand the appearance of Fano resonance in a mechanical system. Indeed, Fano interference is a universal phenomenon because the manifestation of interference does not depend on the matter involved. We will study the appearance of Fano resonance in a linear mechanical

system of coupled oscillators.

1.1 Literature

We first review literature in order to introduce the concept of Fano resonance and its applications.

1.1.1 Background on Fano Resonance

The standard example in a mechanical system where Fano resonance is studied is a system of weakly coupled oscillators, such as one the studied by Joe, et al. (2006). An analogy between a system of coupled oscillators and a system of coupled waves in an electronic wave guide was shown. In this analogy, the interaction between the coupled oscillators is equivalent to interaction between a discrete state and a continuum state of waves with the primary oscillator analogous to the discrete state, and the auxillary oscillator analogous to the continuum state. So, some of the results for Fano resonance in a quantum system are applicable to a mechanical system, and vice versa. For the system of coupled oscillators, the asymmetry in the frequency response curve is caused by the oscillators being out of phase with each other when the forcing frequency passes through the resonant frequency, which then causes the line-shape of the resonance to become distorted due to these sharp variations in the phase. Accordingly, this results in a strong asymmetric line-shape where constructive and destructive effects are located close to each other. With the destructive effect,

the response will vanish, or take on a small value, depending on the strength of the damping effect [2].

In this thesis we shall use an important formulation for Fano resonance presented in B. Luk'yanchuk, et al. (2010).

$$I = \frac{(q\delta + \omega - \omega_0)^2}{(\omega - \omega_0)^2 + \delta^2}, \tag{1.1}$$

where ω is some varying frequency, ω_0 gives the location of the resonance, δ gives the width of the resonance, and I is the intensity of the effect. The parameter q is called the Fano parameter, which gives a measurement for the degree of asymmetry [3]. As q

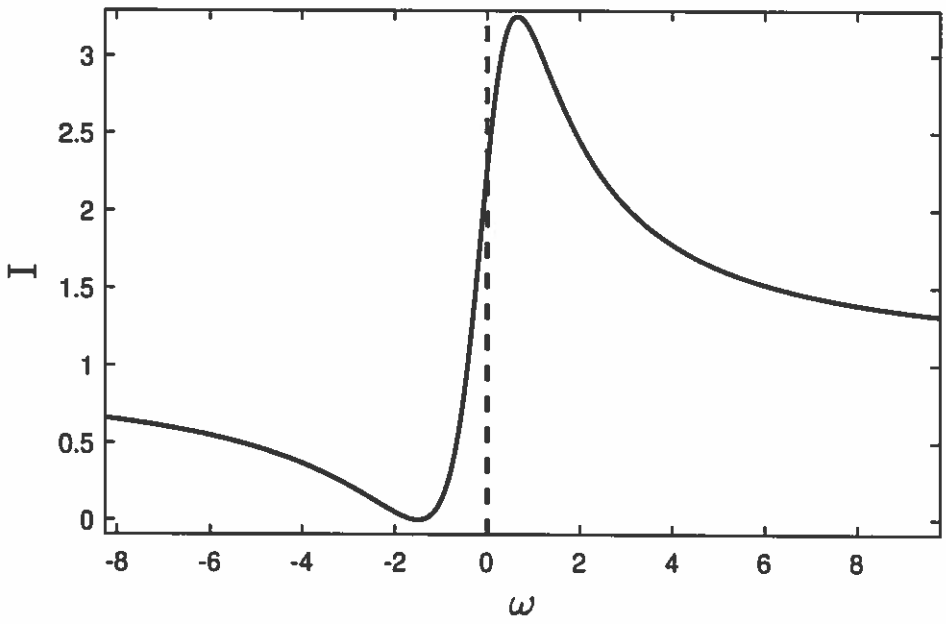

Figure 1.1: Standard example of Fano resonance. This was generated with $q = 1$, $\delta = 1$, and the dashed line shows the location of $\omega_0 = 0$.

goes to 0, the line-shape becomes more asymmetric. If $q = 0$, the line-shape becomes

an anti-resonance (i.e. only the destructive effect is present). And in the extreme case as shown by Q. Wang, et al. (2016) when $q \to \infty$, the resonance reduces to a standard Lorentzian resonance line-shape. In their work, they also showed that the resonances become blurred and broad as the damping effect is increased [4]. Miroshnichenko, et al. (2010) summarized the main charactersitic of a Fano resonance as the asymmetric shape caused by some sort of destructive interference effect, which makes it unique among other resonances. The analysis done also lead to a procedure for locating the location of a Fano resonance. The results showed that in a weakly coupled system, the Fano resonance will appear close to the natural frequencies of the system. This was studied in a quantum description, but can be extended to a mechanical system. In this case, near the lower natural frequency, the response shows a symmetric Lorentzian line-shape, and a Fano resonance appears at the higher natural frequency. We will use this fact later in our analysis of the model, as we only look to study the frequency response where the Fano resonance appears. Also, some theoretical framework for nonlinear Fano resonance in waves was studied. It was found that in general, up to three response branches were found to exist, which results in bistable transmission [5].

1.1.2 Applications

To motivate this work, we will now briefly discuss different applications of Fano resonance. The generic nature of Fano resonance cause it to appear in many different contexts, which leads itself to a variety of applications. Because Fano resonance can

arise from interference between two or more oscillators, its appearance is sensitive to changes in geometry or local enviroment. Thus, small variations can induce dramatic line-shape shifts. This is particularly attractive for a range of applications, with the one of the most straightforward applications of Fano resonant media is the development of chemical and biological sensors [3]. A work done by Chao, et al. (2003) proposed biochemcial sensors that produce a Fano-resonant line-shape with greatly enhanced sensitivity [6]. Also, Lu, et al. (2012) proposed a plasmonic nanosensor based on Fano resonance. The unique features of Fano resonance contributed to a highly efficient sensor for refractive index sensing [7]. J. He, et al. (2016) showed that Fano resonance has applications for developing sensitive tools for single molecular detection and chemical selective imaging, and other nonlinear optical processes [8]. The design of devices able to support Fano resonance is a promising area of research in the fields of plasmonics and nanophotonics, as stated by M. Amin, et al. (2015). In their work, an acoustic device capable of supporting Fano resonance was designed and fabricated to generate acoustically induced transparency by using the cancellation effect seen in Fano resonance [9]. Parallel to plasmonics and metamaterials, progress has been made in the field of nanomechanical systems for ultrasensitive measurements of force and displacement for biosensing and for nanoparticle location. Experimental evidence of Fano resonances in nanomechanical resonators was shown by S. Stassi (2017). In that work, it was shown that the response of a single nanomechanical resonator in an array can show asymmetric peaks characteristic of Fano resonances. This shows that Fano resonances can be experimentally observed in purely mechani-

cal systems, with their example being classical resonators with similar dimensions like nano and microcantilever arrays. These findings provide a new prospective in utilizing the properties of Fano resonance to develop a new generation of nanomechanical sensors with enhanced mass sensitivity [10].

1.2 Summary of Results

Applications for Fano resonance in a purely mechanical system is an emerging field of research, so this work seeks to perform a theoretical study of Fano resonance in a mechanical system using the method of multiple scales. We found that a Fano resonance can appear near the second natural frequency. We then observed how various parameters influenced the strength of the Fano resonance. It was found that decreasing the effect of the damping increased the asymmetry in the resonance line-shape. It was also found that the line-shape became more asymmetric as the locations of the two resonances were squeezed together.

CHAPTER II

LINEAR MODEL

We will analyze how a linear mechanical system displays properties of Fano resonance. We consider a system of coupled oscillators connected by a linear spring and a viscous

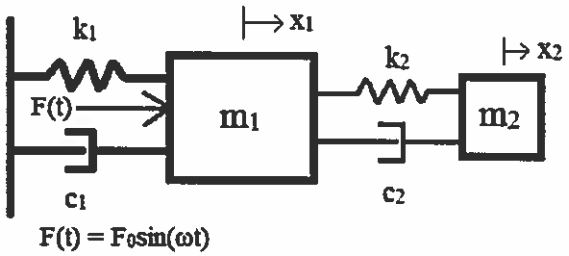

Figure 2.1: Physical model of the oscillators. Here, $m_1 >> m_2$

damper. In this model, we assume the free mass, thought of as an attachment, is much smaller than the larger mass. This fact will be used later when we begin our asymptotic analysis. Figure (2.1) shows a physical model of this system. Note that the dynamics associated with the mass of m_1 is called the primary system, and the dynamics associated with the mass of m_2 is called the auxiliary system.

By applicaition of Newton's 2nd Law, we obtain the differential equations

that govern this system

$$\begin{aligned} m_1\ddot{x}_1 + (c_1+c_2)\dot{x}_1 - c_2\dot{x}_2 + (k_1+k_2)x_1 - k_2x_2 &= F_0\sin(\omega t) \\ m_2\ddot{x}_2 - c_2\dot{x}_1 + c_2\dot{x}_2 - k_2x_1 + k_2x_2 &= 0, \end{aligned} \tag{2.1}$$

where x_1 and x_2 represent the displacement of the masses from their equilibrium positions. In order to simplify this system, we introduce the nondimensional parameters

$$\varepsilon = \frac{m_2}{m_1} \qquad \sigma_1 = \frac{m_1}{m_2}\frac{c_1}{\sqrt{m_1k_1}} \qquad \sigma_2 = \frac{m_1}{m_2}\frac{c_2}{\sqrt{m_1k_1}}$$
$$\kappa = \frac{m_1}{m_2}\frac{k_2}{k_1} \qquad \Omega = \omega\sqrt{\frac{m_1}{k_1}} \qquad \hat{F} = c_x\frac{F_0}{k_1}$$

and the nondimensional variables

$$x = c_x x_1 \quad y = c_x x_2 \quad \tau = \sqrt{\frac{k_1}{m_1}}t \ ,$$

which we will use to nondimensionalize (2.1). Note that the choice for c_x is arbitary and can be any combination that nondimensionalizes x_1 and x_2. Note that $\varepsilon << 1$. To facilitate the analysis to follow, we will assume that the coupling is weakly damped and the system is weakly forced. So, we let $\sigma_2 = \varepsilon\bar{\sigma}_2$ and $\hat{F} = \varepsilon\bar{F}$, where $\bar{\sigma}_2$ and $\bar{F}$ are $O(1)$ quantities. With these choices, the nondimensional equations of motion are

$$\begin{aligned} \ddot{x} + (\varepsilon\sigma_1 + \varepsilon^2\bar{\sigma}_2)\dot{x} - \varepsilon^2\bar{\sigma}_2\dot{y} + (1+\varepsilon\kappa)x - \varepsilon\kappa y &= \varepsilon\bar{F}\sin(\Omega\tau) \\ \ddot{y} - \varepsilon\bar{\sigma}_2\dot{x} + \varepsilon\bar{\sigma}_2\dot{y} - \kappa x + \kappa y &= 0. \end{aligned} \tag{2.2}$$

Because of the presence of linear viscous damping in the system, equation (2.2) can have solutions to which trajectories are attracted to as $t \to \infty$ [11]. We will seek to find these steady-state solutions, and then use them to generate frequency response curves.

2.1 Analysis of Model

First, it will be important to locate the resonances of the frequency response cuve for the primary system. We can calculate this by writing equation (2.2) in matrix form as

$$[M][\ddot{X}] + [\Sigma][\dot{X}] + [K][X] = [F] \tag{2.3}$$

and then solving the associated problem

$$det(-\omega_n^2[M] + [K]) = 0 \tag{2.4}$$

for ω_n, the natural frequencies of the system. Equation (2.4) will have two solutions

$$\begin{aligned} \omega_{n_1} &\approx 1 \\ \omega_{n_2} &\approx \sqrt{\kappa}. \end{aligned} \tag{2.5}$$

As stated in section 1.1.1, Fano resonance can appear near ω_{n_2}, and near ω_{n_1}, a standard Lorentzian resonance will appear.

2.1.1 Multiple Scales Analysis

Due to the presence of different time-scales associated with this system, we will employ the method of multiple scales to analyze the system's behavior. First, we introduce the frequency detuning

$$\Omega = \sqrt{\kappa} + \varepsilon\gamma$$

which will allow us to capture the behavior of the system near the Fano resonance. The parameter γ is called the frequency detuning parameter, and it quantitatively

describes how close exictation frequency is to the resonant frequency. In the perturbation anaylsis to follow we will track terms up to $O(\varepsilon)$, and by introducing the frequency detuning we will be able to easier reconginze the terms that lead to secular terms. To apply the method of multiple scales we assume the expansions

$$\begin{aligned} x &= x_0 + \varepsilon x_1 + ... \\ y &= y_0 + \varepsilon y_1 + ... \\ \eta_0 &= \Omega\tau \\ \eta_1 &= \varepsilon\Omega\tau. \end{aligned} \tag{2.6}$$

With these assumptions, we find that

$$\begin{aligned} \tfrac{d}{d\tau} &= \Omega(D_0 + \varepsilon D_1) \\ \tfrac{d^2}{d\tau^2} &= \Omega^2(D_0^2 + 2\varepsilon D_0 D_1), \end{aligned} \tag{2.7}$$

where D_0 denotes $\frac{\partial}{\partial\eta_0}$ and D_1 denotes $\frac{\partial}{\partial\eta_1}$. After applying this change of variables to (2.2) and collecting like powers of ε, we obtain the perturbation hierarchy

$O(1)$:

$$\kappa D_0^2 x_0 + x_0 = 0 \tag{2.8}$$

$$D_0^2 y_0 + y_0 = x_0 \tag{2.9}$$

$O(\varepsilon)$:

$$\kappa D_0^2 x_1 + x_1 = -2\sqrt{\kappa}\gamma D_0^2 - 2\kappa D_0 D_1 - \sigma_1\sqrt{\kappa} D_0 x_0 - \kappa x_0 + \kappa y_0 + \bar{F}\sin(\eta_0) \tag{2.10}$$

$$D_0^2 y_1 + y_1 = -\frac{2\gamma}{\sqrt{\kappa}} D_0^2 y_0 - 2D_0 D_1 y_0 + \frac{\bar{\sigma_2}}{\sqrt{\kappa}} D_0 x_0 - \frac{\bar{\sigma_2}}{\sqrt{\kappa}} D_0 y_0 + x_1. \tag{2.11}$$

Equations (2.8) through (2.11) can be solved in order. We find that

$$x_0 = A_0(\eta_1)\sin\left(\frac{1}{\sqrt{\kappa}}\eta_0\right) + B_0(\eta_1)\cos\left(\frac{1}{\sqrt{\kappa}}\eta_0\right), \tag{2.12}$$

where A_0 and B_0 are to be determined. Now that we have the solution for x_0, we can find the solution to (2.9). Equation (2.9) has homogeneous solution

$$y_{0,h} = U_0(\eta_1)\sin(\eta_0) + V_0(\eta_1)\cos(\eta_0),$$

where U_0 and V_0 are to be determined. The particular solution to (2.9) is

$$y_{0,p} = -\frac{\kappa}{\kappa-1}A_0 \sin\left(\frac{1}{\sqrt{\kappa}}\eta_0\right) - \frac{\kappa}{\kappa-1}B_0\cos\left(\frac{1}{\sqrt{\kappa}}\eta_0\right).$$

So, the solution to (2.9) is given by

$$y_0 = y_{0,h} + y_{0,p}. \tag{2.13}$$

Next we can insert (2.12) and (2.13) into (2.10) in order to solve for x_1. Before solving for x_1, we must remove the possibility of secular terms in the solutions by setting the sources of these terms equal to 0. In this case the sources of the secular terms will be the ones with frequency $\frac{1}{\sqrt{\kappa}}$. After doing so we obtain two equations for A_0 and B_0

$$\begin{aligned} D_1 A_0 &= -\tfrac{1}{2}\tfrac{\sigma_1}{\sqrt{\kappa}}A_0 + \left(\gamma - \tfrac{1}{2}\tfrac{\kappa^{3/2}}{\kappa-1}\right)B_0 \\ D_1 B_0 &= -\left(\gamma - \tfrac{1}{2}\tfrac{\kappa 3/2}{\kappa-1}\right)A_0 - \tfrac{1}{2}\tfrac{\sigma_1}{\sqrt{\kappa}}B_0. \end{aligned} \tag{2.14}$$

Since we are looking for the steady-state solution, we look to find fixed points of (2.14). The only fixed point of this system is $A_0 = 0$ and $B_0 = 0$. Note that since the eigenvalues associated with this system given by

$$\lambda = -\frac{1}{2}\frac{\sigma_1}{\sqrt{\kappa}} \pm \frac{1}{2}\sqrt{-\frac{3}{4}\left(\frac{\sigma_1}{\sqrt{\kappa}}\right)^2 - 4\left(\gamma - \frac{1}{2}\frac{\kappa^{3/2}}{\kappa-1}\right)^2}$$

are complex with negative real part, the trajectories behave as stable spirals attacted to the origin. So, we simply set $A_0 = 0$ and $B_0 = 0$. With that completed we now

have

$$x_0 = 0 \tag{2.15}$$

$$y_0 = U_0(\eta_1)\sin(\eta_0) + V_0\cos(\eta_0). \tag{2.16}$$

After the sources of the secular terms in (2.10) are removed and (2.15) and (2.16) are inserted into (2.10), we find that x_1 will satisfy

$$\kappa D_0^2 x_1 + x_1 = \kappa U_0 \sin(\eta_0) + \kappa V_0 \cos(\eta_0). \tag{2.17}$$

Following a similar procedure as the one done for x_0 shows that the homogeneous solution to (2.17) goes to 0 in the steady-state. This is due to the presence of linear viscous damping in the system, which causes the transient response (in the form of the homogeneous solution) to decay to 0 in the steady-state. So, we simply search for a particular solution to (2.17), which is given by

$$x_1 = -\frac{\kappa}{\kappa-1}U_0\sin(\eta_0) - \frac{\kappa}{\kappa-1}V_0\cos(\eta_0) - \frac{\bar{F}}{\kappa-1}\sin(\eta_0). \tag{2.18}$$

The next step is to move to (2.11), which we will not solve because we are only interested in the response of the primary system. However, by removing the sources of the secular terms, we can find equations for U_0 and V_0. Pieces with frequency 1 will cause secular terms in the solution for y_1, so we set them equal to zero. This results in the equations

$$\begin{aligned} D_1 U_0 &= -\tfrac{1}{2}\tfrac{\bar{\sigma}_2}{\sqrt{\kappa}}U_0 + \left(\tfrac{\gamma}{\sqrt{\kappa}} - \tfrac{1}{2}\tfrac{\kappa}{\kappa-1}\right)V_0 \\ D_1 V_0 &= -\left(\tfrac{\gamma}{\sqrt{\kappa}} - \tfrac{1}{2}\tfrac{\kappa}{\kappa-1}\right)U_0 - \tfrac{1}{2}\tfrac{\bar{\sigma}_2}{\sqrt{\kappa}}V_0 - \tfrac{1}{2}\tfrac{\bar{F}}{\kappa-1}. \end{aligned} \tag{2.19}$$

Similar to the analysis for A_0 and B_0, the presence of damping in the system will mean that the transient response will decay to 0. Thus, we seek a steady-state solution, so

we look for the fixed points of (2.19). By setting $D_1 U_0 = 0$ and $D_1 V_0 = 0$, we obtain the equations

$$\begin{aligned} -\tfrac{1}{2}\bar{\sigma}_2 U_0 + \left(\gamma - \tfrac{1}{2}\tfrac{\kappa^{3/2}}{\kappa-1}\right) V_0 &= 0 \\ -\left(\gamma - \tfrac{1}{2}\tfrac{\kappa^{3/2}}{\kappa-1}\right) U_0 - \tfrac{1}{2}\bar{\sigma}_2 V_0 &= \tfrac{1}{2}\tfrac{\sqrt{\kappa}}{\kappa-1}\bar{F}. \end{aligned} \tag{2.20}$$

The solution to (2.20) is given by

$$U_0 = \frac{-\sqrt{\kappa}}{2(\kappa-1)} \frac{\bar{F}}{\left(\gamma - \frac{1}{2}\frac{\kappa^{3/2}}{\kappa-1}\right)^2 + \left(\frac{\bar{\sigma}_2}{2}\right)^2} \tag{2.21}$$

$$V_0 = \frac{-\sqrt{\kappa}}{4(\kappa-1)} \frac{\bar{\sigma}_2 \bar{F}}{\left(\gamma - \frac{1}{2}\frac{\kappa^{3/2}}{\kappa-1}\right)^2 + \left(\frac{\bar{\sigma}_2}{2}\right)^2}. \tag{2.22}$$

Since we are only interested in the response of the primary system, we do not seek to solve (2.11).

We have now discovered that the mutliple scales approximation to the steady-state response of the primary system is $x = \varepsilon x_1$, where x_1 is given by (2.18) when (2.21) and (2.22) are inserted. In order to better understand the steady-state behavior, we rewrite the approximation for x in the form

$$x = X \sin(\eta_0 + \phi), \tag{2.23}$$

where the amplitude X is given by

$$X = \varepsilon \sqrt{\left(\frac{\kappa}{\kappa-1} U_0 + \frac{\bar{F}}{\kappa-1}\right)^2 + \left(\frac{\kappa}{\kappa-1} V_0\right)^2}, \tag{2.24}$$

and the phase shift ϕ is given by

$$\phi = \tan^{-1}\left(\frac{\kappa U_0 + \bar{F}}{\kappa V_0}\right). \tag{2.25}$$

In order to analyze the Fano-resonant behavior of the system, we first note that by letting

$$r = \gamma - \tfrac{1}{2}\tfrac{\kappa^{3/2}}{\kappa-1}$$

$$\delta = \tfrac{\sigma_2}{2},$$

equation (2.24) can alternatively be expressed as

$$X = \varepsilon \frac{\bar{F}}{(\kappa-1)^2} \frac{\sqrt{(\kappa-1)\left(r^2+\delta^2\right)^2 + \left(\kappa^{3/2}(\kappa-1)r + \tfrac{1}{4}\kappa^3\right)\left(r^2+\delta^2\right)}}{r^2+\delta^2} \tag{2.26}$$

First, let $g(\gamma)$ denote the numerator of (2.26). Then, we will capture the Fano-resonant properties of the frequency-response curve by fitting (2.26) to a curve of the form

$$X_{Fano} = \varepsilon \frac{\bar{F}}{(\kappa-1)^2} \frac{\left(q\delta + \gamma - \tfrac{1}{2}\tfrac{\kappa^{3/2}}{\kappa-1}\right)^2}{\left(\gamma - \tfrac{1}{2}\tfrac{\kappa^{3/2}}{\kappa-1}\right)^2 + \delta^2}, \tag{2.27}$$

where the Fano parameter q will be determined by numerical curve fitting. In order to find the best approximation to (2.26) of the form (2.27), we find a q which minimizes the difference between the two curves in the L_2-norm. So, q satisfies

$$q = arg\,min_q \int_{\gamma^-}^{\gamma^+} \left(X - X_{Fano}(q)\right)^2 d\gamma, \tag{2.28}$$

where γ^- and γ^+ are the endpoints of some interval we wish to approximate (2.26) in. By properties of derivatives, the best approximation can equivalently be found by find a value of q which satisfies

$$\frac{d}{dq} \int_{\gamma^-}^{\gamma^+} \left(X - X_{Fano}(q)\right)^2 d\gamma = 0. \tag{2.29}$$

Because both X and X_{Fano} are continuous and their derivatives with respect to q are continuous, we can pass the derivative through the integral. After doing so, we see

that q will satisfy the root-finding problem

$$I_1(q) - \delta I_2 q - I_3 = 0, \tag{2.30}$$

where

$$I_1(q) = \int_{\gamma^-}^{\gamma^+} \frac{\left(q\delta + \left(\gamma - \frac{1}{2}\frac{\kappa^{3/2}}{\kappa-1}\right)^2\right)^3}{\left(\left(\gamma - \frac{1}{2}\frac{\kappa^{3/2}}{\kappa-1}\right)^2 + \delta^2\right)^2} d\gamma$$

$$I_2 = \int_{\gamma^-}^{\gamma^+} \frac{g(\gamma)}{\left(\left(\gamma - \frac{1}{2}\frac{\kappa^{3/2}}{\kappa-1}\right)^2 + \delta^2\right)^2} d\gamma$$

$$I_3 = \int_{\gamma^-}^{\gamma^+} \frac{g(\gamma)\left(\gamma - \frac{1}{2}\frac{\kappa^{3/2}}{\kappa-1}\right)}{\left(\left(\gamma - \frac{1}{2}\frac{\kappa^{3/2}}{\kappa-1}\right)^2 + \delta^2\right)^2} d\gamma.$$

To evaluate these integrals, we will numerically integrate I_2 and I_3. The integral I_1 has an exact form, which can be found in [list any handbook]. Then, equation (2.30) is numerically minimized to find the value of q which finds the best approximation to (2.26) in the form (2.27).

The frequency response curves generated by (2.26) are shown in Figure (2.2) for various strengths of the damping effect, $\bar{\sigma}_2$. Here, we can see that certain properties of Fano resonance appear. Namely, an anti-resonance appears close to a normal resonance condition. This means that the system can go from a state of low amplitude to high amplitude with a very small change in the forcing frequency. We can also observe that as the strength of the damping effect increases, the effect of the resonance decreases.

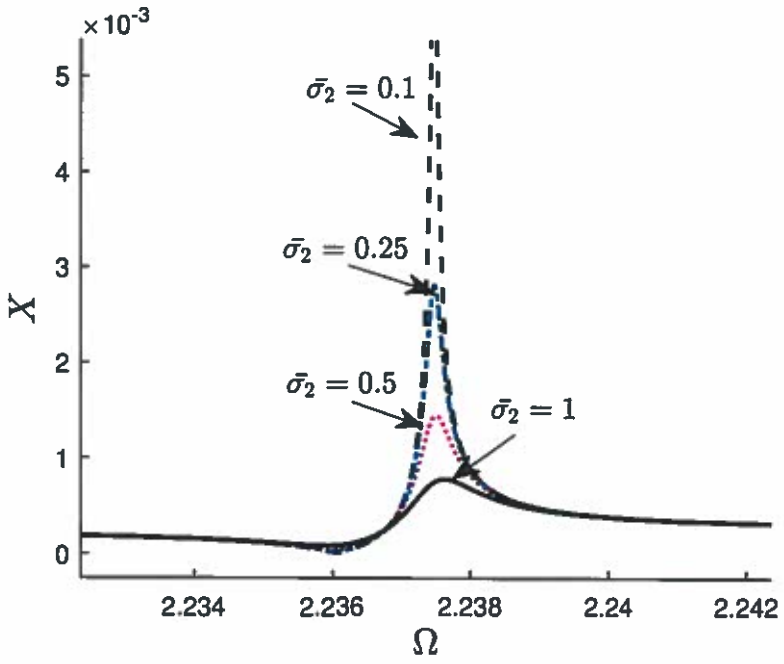

Figure 2.2: Frequency response plots for various strenghts of damping, $\bar{\sigma}_2$. The parameters values used to generate these curves are $\varepsilon = 0.001$, $\kappa = 5$, and $\bar{F} = 1$.

In a purely mechanical system, such as the one we are studying, we can interpret the asymmetry in the system as the distance between the resonance and anti-resonance. If the resonance and anti-resonance are close together, then the system can switch between high and low amplitudes with a relatively small change in the forcing frequency. So, squeezing these together will result in a more asymmetric response, as this effect will become more apparent. The advantage of using curves in the form of (2.27) is that $q\delta$ will give us a way to measure that distance. This is because the anti-resonance appears when the numerator is minimized. So, the line-shape is more asymmetric when $q\delta$ is relatively small because the resonance and anti-resonance

are closer together, and if $q\delta$ is relatively large the resonance and anti-resonance are spread out, leading to a more symmetric line-shape.

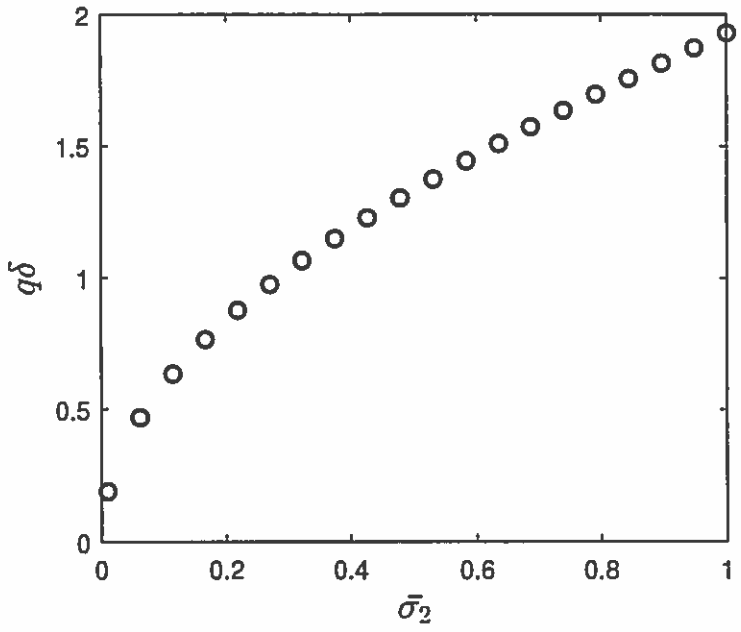

Figure 2.3: Values of $q\delta$ for various strengths of the damping effect, $\bar{\sigma}_2$. The parameter values used to generate these are $\varepsilon = 0.001$, $\kappa = 5$, and $\bar{F} = 1$. Here, we used $\gamma^- = -10$ and $\gamma^+ = 10$.

In Figure (2.3), we observe how $q\delta$ varies depending on the damping. As stated before, the lower the value of $q\delta$ becomes, the more asymmetric the resonance line-shape becomes. So, we see that as the effect of the damping is decreased, the more asymmetric the line-shape becomes. This is also evident in Figure (2.2) where we see smaller values of $\bar{\sigma}_2$ lead to more asymmetric shapes, in the sense that the difference between the resonance amplitude and anti-resonance amplitude grows. We also see the role that κ plays in the asymmetry in Figure (2.4). Here, we find that

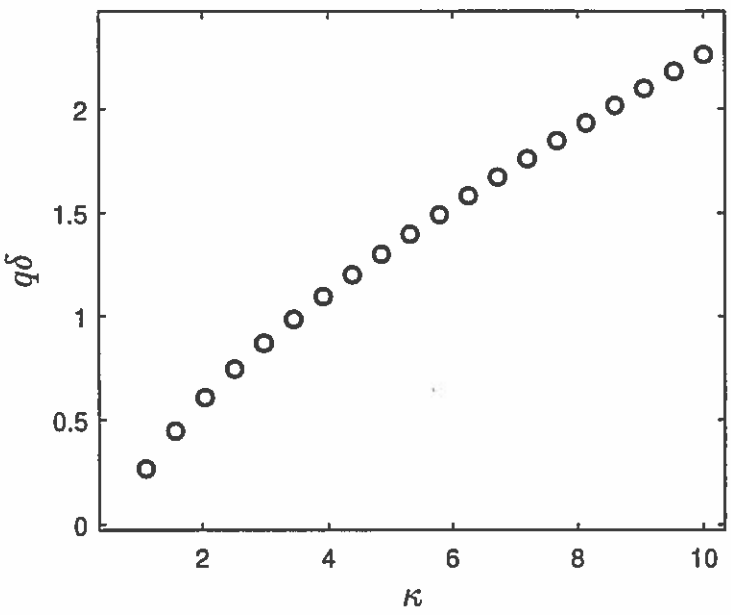

Figure 2.4: Values of $q\delta$ for various strengths of κ. The parameter values used to generate these are $\epsilon = 0.001$, $\bar{\sigma_2} = 0.5$, and $\bar{F} = 1$. Here, we used $\gamma^- = -10$ and $\gamma^+ = 10$.

as the value of κ becomes closer to 1 (when the Fano resonance gets closer to the Lorentzian resonance), the more asymmetric the line-shape becomes.

In Figure (2.5), we show one case of fitting X_{Fano} to X. We see that the curve is a relatively good fit, because the approximation captures the imporant charateristics of the system.

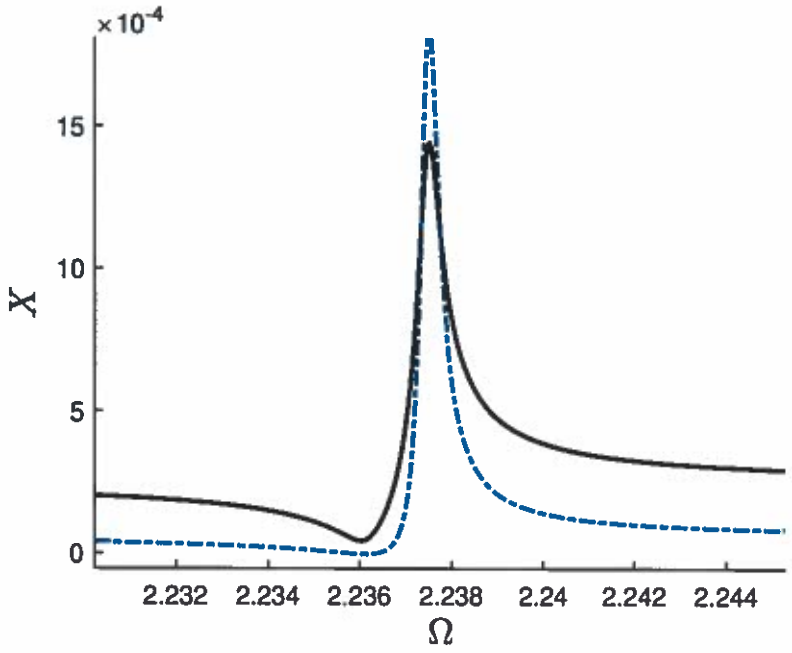

Figure 2.5: A comparison of X to the curve-fitted approximation X_{Fano}. The parameters used to generate these curves are $\varepsilon = 0.001$, $\kappa = 5$, $\bar{\sigma}_2 = 0.5$, and $\bar{F} = 1$. We also find $q = 5.33$

CHAPTER III

SUMMARY OF RESULTS

We studied the appearance of Fano resonance in a purely mechanical system. We found that a Fano resonance can appear near the second natural frequency of the system under certain conditions. Then, the way the various parameters influence the Fano resonance were studied. Using curve fitting, we were able to compare the multiple-scales approximation to an equation in the generic Fano resonance form. It was found that decreasing the effect of the damping seems to increase the asymmetry in the resonance line-shape. Also, the closer the natural frequenices become, the more asymmetric the line-shape becomes. Because the appearance of Fano resonances in purely mechanical systems is an emerging field of research, this work hopes to provide some theoretical background on this topic. In a further work, we will study the appearance of Fano resonances in a nonlinear mechanical system, and that work will be built off of these results.

BIBLIOGRAPHY

[1] U. Fano. Effects of configuration interaction on intensities and phase shifts. *American Physical Society*, 124:1866–1878, 1961.

[2] Y. Joe, A. Satanin, and C. Kim. Classical analogy of fano resonances. *Physica Scripta*, 74, 2006.

[3] B. Luk'yanchuk et. al. The fano resonance in plasmonic nanostructures and metamaterials. *Nature Materials*, 9:707–715, 2010.

[4] Q. Wang et. al. Analysis of transition from lorentz resonance to fano resonance in plasmon and metamaterial systems. *Optical and Quantum Electronics*, 48, 2016.

[5] Andrey E. Miroshnichenko, Sergej Flach, and Yuri S. Kivshar. Fano resonances in nanoscale structures. *Reviews of Modern Physics*, 82:2257–2298, 2010.

[6] C. Chao and L.J. Guo. Biochemical sensors based on polymer microrings with sharp asymmetrical resonance. *Applied Physics Letters*, 83:1527, 2003.

[7] H. Lu, D. Mao, and G. Wang. Plasmonic nanosensor based on fano resonance in waveguide-coupled resonators. *Optics Letters*, 37:3780–3782, 2012.

[8] J. He et. al. Near-field engineering of fano resonances in a plasmonic assembly for maximizing cars enhancements. *Scientific Reports*, 6, 2016.

[9] M. Amin et. al. Acoustically induced transparency using fano resonant periodic arrays. *Journal of Applied Physics*, 118, 2015.

[10] S. Stassi et. al. Experimental evidence of fano resonances in nanomechanical resonators. *Scientific Reports*, 7, 2017.

[11] T. Kalmar-Nagy and B. Balachandran. Forced harmonic vibration of a duffing oscillator with linear viscous damping. 2011.